EXPERIMENTS WITH A CONTINUUM ROBOT STRUCTURE

Dorian Cojocaru, Sorin Dumitru, Florin Manta, Giuseppe Boccolato
Faculty of Automation, Computers and Electronic, University of Craiova, Bld. Decebal, Craiova, Romania

Ion Manea
Faculty of Mechanics, University of Craiova, Calea Bucuresti Str., Craiova, Romania

Keywords: Continuum Robots, Kinematics, Mechanical Experiments.

Abstract: A continuum arm prototype was designed and implemented using two different shapes: cylinder like and cone like. This new robot is actuated by stepper motors. The rotation of these motors rotates the cables which by correlated screwing and unscrewing of their ends determine their shortening or prolonging, and by consequence, the tentacle curvature. The kinematics and dynamics models, as well as the different control methods developed by the research group were tested on these robots. The lack of no discrete joints is a serious and difficult issue in the determination of the robot's shape. A solution for this problem is the vision based control of the robot, kinematics and dynamics. An image – based visual servo control where the error control signal is defined directly in terms of image feature parameters was designed and implemented. In this paper, we analyze some mechanical capabilities of this type of continuous robots. We present the structure of the tentacle robot, it's kinematics model and the results for a series of tests regarding the mechanical behaviour of the robotic structure.

1 INTRODUCTION

Modern industrial robots are mostly (human) arm-inspired mechanisms with serially arranged discrete links. When it comes to industrial environment where the workspace is structured and predefined this kind of structure is fine. This type of robots are placed in carefully controlled environments and kept away from human and their world.

When it comes to robots that must interact with the natural world, it needs to be able to solve the same problems that animals do. The rigid structure of traditional robots limit their ability to maneuver and in small spaces and congested environments, and to adapt to variations in their environmental contact conditions (Suzumori et al., 1991), (Robinson and Davies, 1999). For improving the adaptability and versatility of robots, recently there has been interest and research in "soft" robots (Cowan and Walker, 2008). In particular, several research groups are investigating robots based on continuous body "continuum" structure. If a robot's body is soft and/or continuously bendable it might emulate a snake or an eel with an undulating locomotion (Crespi and Ijspeert, 2006).

The continuum or hyper-redundant robot manipulators behaviour is similar to biological trunks, tentacles or snakes. The movement of the continuum robot mechanisms is generated by ending continuously along their length to produce a sequence of smooth curves (Blessing and Walker, 2004). This contrasts with discrete robot devices, which generate movement at independent joints separated by supporting links.

We can also describe as continuum robots snake-like robots and elephant's trunk robots, although these descriptions are restrictive in their definitions and cannot be applied to all snake-arm robots. A continuum robot is a continuously curving manipulator, much like the arm of an octopus (Davies, J.B.C., 1998). An elephant's trunk robot is a good descriptor of a continuum robot. The elephant's trunk robot has been generally associated with an arm manipulation – an entire arm used to grasp and manipulate objects, the same way that an elephant would pick up an apple. Snake-arm robots are often used in association with another device meant to introduce the snake-arm into the confined space. However, the development of high-

Cojocaru D., Dumitru S., Manta F., Boccolato G. and Manea I. (2010).
EXPERIMENTS WITH A CONTINUUM ROBOT STRUCTURE.
In *Proceedings of the 7th International Conference on Informatics in Control, Automation and Robotics*, pages 198-205
DOI: 10.5220/0002921501980205

performance control algorithms for these manipulators is quite a challenge, due to their unique design and the high degree of uncertainty in their dynamic models. The great number of parameters, theoretically an infinite one, makes very difficult the use of classical control and the conventional transducers for position and orientation.

2 THE ROBOTIC STRUCTURE

A research group from the Faculty of Automation, Computers and Electronics, University of Craiova, Romania, started working in research field of hyper redundant robots over 20 years ago. The experiments started on a family of TEROB robots which used cables and DC motors. The kinematics and dynamics models, as well as the different control methods developed by the research group were tested on these robots. Since 2008, the research group designed a new experimental platform for hyper redundant robots.

Our robotic system is composed from two units, one with a flexible structure with kinematic possibilities similar with the snake's locomotion and another one with driving. The flexible unit is composed from three modules with independent driving, that confers a complex 3D configuration, with multiple kinematic possibilities for the working space. The flexible structure is conceived in modular systems with decoupling possibilities for a controlled optimization of the working space.

The flexible structure as an integrate system, or as independent modules, is conceived to allow driving in two modes, respective:

- one with wires and a flexible central column;
- one with flexible vertebrates and a flexible central column;

In the case where the driving is made by wires, a module has two freedom degrees and in the case of driving with flexible columns each module has three degrees of freedom. As it can be observed the flexible unit structured in three modules for controlling a complex workspace, with multiple kinematic possibilities. The machine structure for each module is based upon thread transmissions with self decelerations possibilities and adjust of the axial-radial clearances.The flexible unit with the snake-like design is composed from a base flange, some intermediary flanges, and four flexible shafts, with high elasticity, which will be called vertebral spines. The central shaft is mounted rigidly to all the intermediary flanges, fig. 1.

The three super elastic spines are mounted equidistantly upon the central spine. The entire vertebrates are connected only to the end flange. The intermediary flanges maintain constant the radial distance between the secondary tubes and the central vertebrate. Changing in an active way the length for two of the vertebrate spines, the final flange can be manipulated with two degrees of freedom in any direction.

The three actuating spines are rigidly jointed only to the end flange, the joint between them and the intermediary flanges is like one translational joint.

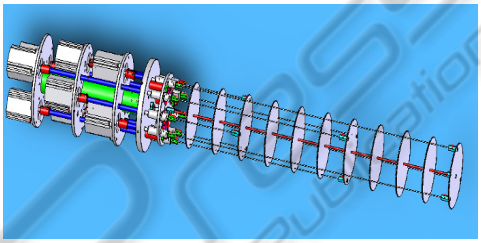

Figure 1: The virtual model with the driving and vertebral unit.

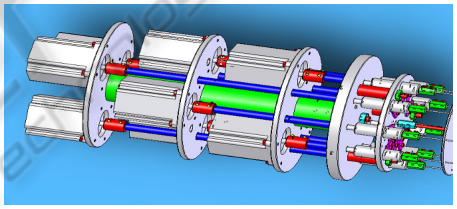

Figure 2: Redundant driving unit.

Figure 3: The assembly of the robotic system with the baggy vertebral unit.

2.1 Experimental Modelling

As it was presented above, the robot is designed in a modular structure, with three modules, independently actuated through thread transmissions with possibility to adjust the radial and axial clearances, in the aim to assure the imposed kinematics precision. The vertebrate unit is designed to work in two ways, respectively with two or three degrees of freedom on each module.

2.2 Modelling with Finite Elements

For demonstrating the viability of mechanical system it is proposed the modelling and simulation functionality with finite element method. Faithfully are respected the shape conditions and loadings, so that through a Virtual Prototyping attempt it is obtained a parameterized virtual system, which can be loaded so that you get various types of deformed shapes, obviously controlled for the analyzed mechanic system (Dumitru et al., 2009).

Parameterized modelling of the flexible system allows 3D simulation for different variants with one, two or three modules, with different size dimensions and types of materials with circular vertebras full or tubular, in this way assuring a wider area of skills for the proposed and analyzed system.

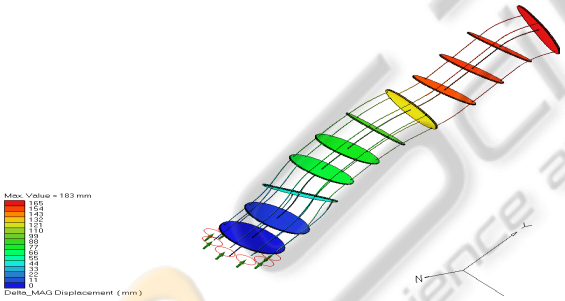

Figure 4: Elastic displacement distribution for a kinematic chain with 3 modules.

3 THE KINEMATIC MODEL OF THE TENTACLE ARM

In order to control a hyper-redundant robot we have to develop a method to compute the positions for each one of his segments (Ivanescu et al., 2006). By consequence, given a desired curvature S*(x, tf) as sequence of semi circles, identify how to move the structure, to obtain s(x, t) such that:

$$\lim_{t \to t_f} s(x,t) = S^*(x,t_f) \quad (1)$$

where x is the column vector of the shape description and tf is the final time (see Fig. 6).

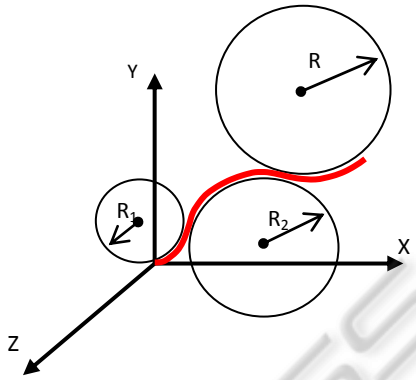

Figure 5: The description of the desired shape.

3.1 Tentacle Shape Description

The tentacle's shape will be described considering two angles (θ, α) for each segment, where θ is the rotation angle around Z-axis and is the rotation angle around the Y-axis (see Figure 5). In order to describe the movement we can use the roto-translation matrix as shown in Figure 6. Figure 7 shows the relation between the orientation of one projection on the main plane segment and the curvature angle of the previous segment.

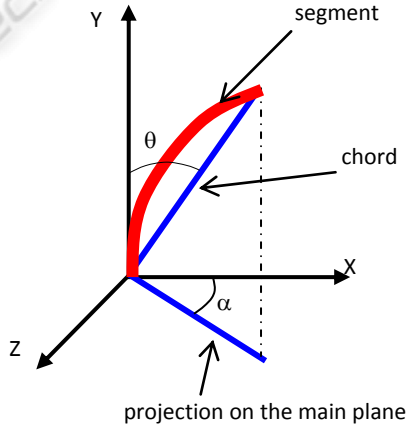

Figure 6: The description of a 3D curvature.

$$\begin{bmatrix} cos(2\cdot\beta) & sin(2\cdot\beta) & L\cdot sin(\beta) \\ -sin(2\cdot\beta) & cos(2\cdot\beta) & L\cdot cos(\beta) \\ 0 & 0 & 1 \end{bmatrix} \quad (2)$$

The generic matrix in 2D that expresses the coordinate of the next segment related to the previous reference system can be written as follow:

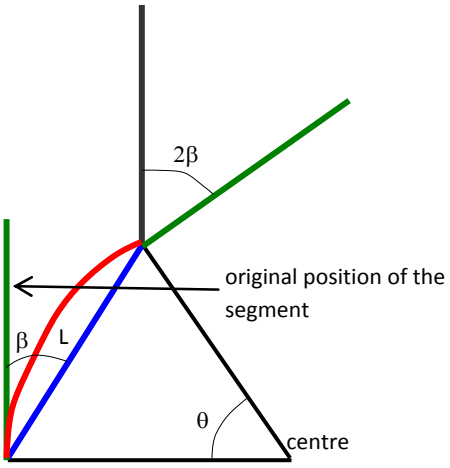

Figure 7: Curvature and relation between θ and β.

In 3D space we cannot write immediately the dependence that exists between segments. This relation can be obtained through the pre-multiplication of generic roto-translation matrix (Cojocaru et al., 2008). One of the possible combinations to express the coordinate of the next segment related to the frame coordinate of the previous segment is the following:

$$R^i_{generic} := R^i_z(\theta^i) \cdot Tr_y(V^i) \cdot R^i_y(\alpha^i) \cdot R^i_z(\theta^i) \quad (3)$$

where $R^i_z(\theta^i)$ and $R^i_y(\alpha^i)$ are the fundamental roto-translation matrix having 4x4 elements in 3-D space, and Try(V) is a 4x4 elements matrix of pure translation in 3-D space and where Vi is the vector describing the translation between two segments expressed in coordinate of i-th reference system. The main problem remains to obtain an imposed shape for the tentacle arm. In order to control the robot, we need to obtain the relation between the position of the wires and the position of the segment.

3.2 Curvature of One Segment

In the current stage of our research, a decoupled approach is used for the robot control scheme, thus the three segments are controlled separately, without considering the interaction between them. This section presents the way direct kinematics of one segment was obtained. The geometry of one segment for the 2D case is described in Fig. 10. The curvature angle θ of the segment is considered as the input parameter, while the lengths L1 and L2 of the control wires are the outputs (Boccolato et all., 2009).

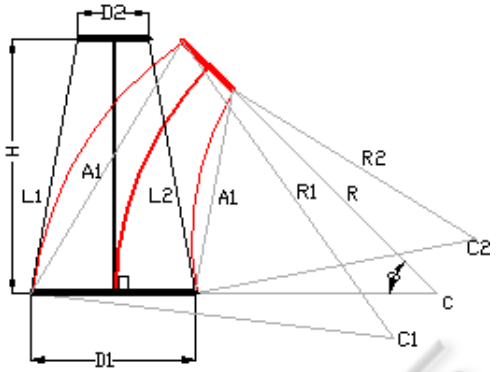

Figure 8: The geometry of one segment.

The radius R of the segment curvature is obtained using equation (4):

$$R = \frac{H}{\theta} \quad (4)$$

where H is the height of the segment. The following lengths are obtained from Fig. 10, based on the segment curvature:

$$L_{11} = R + \frac{D_1}{2} \qquad L_{12} = R + \frac{D_2}{2}$$
$$L_{21} = R - \frac{D_1}{2} \qquad L_{22} = R - \frac{D_2}{2} \quad (5)$$

where D1 and D2 are the diameters of the segment end discs.
Based on the Carnot theorem, the lengths A1 and A2 are then obtained:

$$A_1 = \sqrt{L_{11}^2 + L_{12}^2 - 2 \cdot L_{11}^2 \cdot L_{12}^2 \cdot \cos\theta}$$
$$A_2 = \sqrt{L_{21}^2 + L_{22}^2 - 2 \cdot L_{21}^2 \cdot L_{22}^2 \cdot \cos\theta} \quad (6)$$

The control wires curvature radius R1 and R2 are given by the relations (7):

$$R_1 = \frac{A_1}{2 \cdot \sin\frac{\theta}{2}} \qquad R_2 = \frac{A_2}{2 \cdot \sin\frac{\theta}{2}} \quad (7)$$

Finally, the lengths of the control wires are obtained as in (8):

$$L_{w1} = R_1 \cdot \theta = \frac{A_1 \cdot \theta}{2 \cdot \sin\frac{\theta}{2}}$$
$$L_{w2} = R_2 \cdot \theta = \frac{A_2 \cdot \theta}{2 \cdot \sin\frac{\theta}{2}} \quad (8)$$

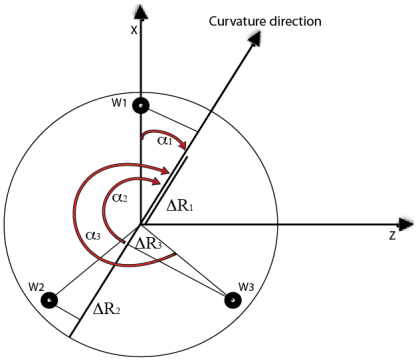

Figure 9: Projection of the wire to get the α direction.

For the 3D case, a virtual wire is considered, which gives the α direction of the curvature. Considering one virtual wire in the direction of the desired curvature having length calculated as below. First, the following lengths are calculated:

$$\begin{aligned} L_{11} &= R + \frac{D_1}{2}\cdot cos(\alpha_1) \quad L_{12} = R + \frac{D_2}{2}\cdot cos(\alpha_1) \\ L_{21} &= R + \frac{D_1}{2}\cdot cos(\alpha_2) \quad L_{22} = R + \frac{D_2}{2}\cdot cos(\alpha_2) \\ L_{31} &= R + \frac{D_1}{2}\cdot cos(\alpha_3) \quad L_{22} = R + \frac{D_2}{2}\cdot cos(\alpha_3) \end{aligned} \tag{9}$$

$$\begin{cases} \alpha_1 = -\alpha \\ \alpha_2 = 120° - \alpha \\ \alpha_3 = 240° - \alpha \end{cases} \tag{10}$$

Based on (6) and (9) the curvature radius R1, R2 and R3 of the three control wires are then obtained. Finally the lengths of the control wires are calculated with relation (11):

$$\begin{aligned} L_{w1} &= R_1 \cdot \theta \\ L_{w2} &= R_2 \cdot \theta \\ L_{w3} &= R_3 \cdot \theta \end{aligned} \tag{11}$$

Besides, for the system presented we can obtain two useful relations:

$$\begin{cases} \sum_{i=1}^{3} \cos(\alpha_i) = 0 \\ \frac{1}{3}\sum_{i=1}^{3} Lw_i = L \end{cases} \tag{12}$$

The second equation can be utilized to estimate the compression or the extension of the central bone.

4 EXPERIMENTS

We conducted a series of experiments, having as purpose the analysis of the robotic structure, including the behavior of the arm and the stepper motors used for its actuation.

For these tests, we used the following equipment:

- Spider 8 acquisition system, with eight input channels and 12 bit resolution per channel
- Nexus 2692-A-0I4 signal conditioner with load compensation, four input/output channels, frequency domain 0.1Hz ÷ 100KHz and linearity error ≤0.05%;
- Bruel&Kjaer model 4391 accelerometers, frequency domain 0.3 ÷ 10000Hz, load 1 pC/ms-2, linearity error ≤1%;

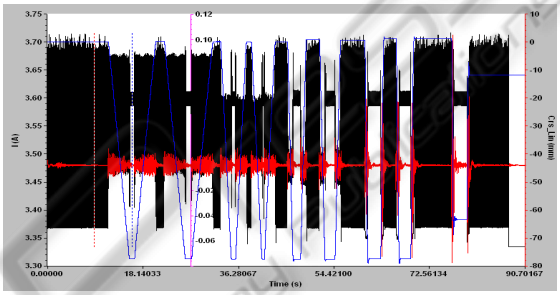

Figure 10: Recorded dataset. Marked with black - the current, with red - end effector oscillation and with blue - the displacement.

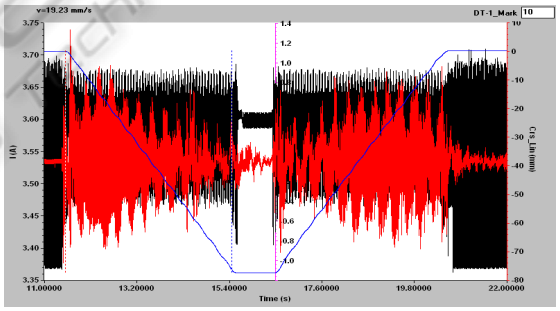

Figure 11: Recorded data for a movement executed at 19.23 mm/s.

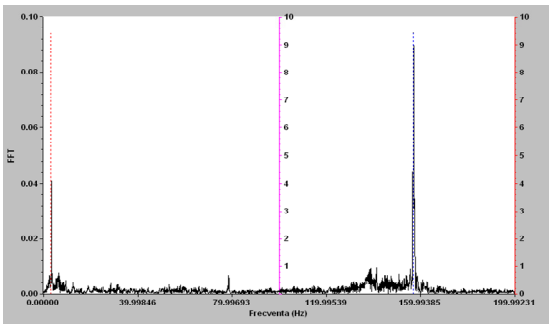

Figure 12: Frequency analysis for oscillation. Slow speed case.

- WA300 inductive transducer for linear displacement, displacement range 0÷300mm, linearity error ≤1%;
- MicroSwitch model CSLA 20KI current transducer, current domain ±20A, linearity error ≤1%
- The data was recorded on a IBM notebook with Testpoint V5.1 soft-ware installed

We placed the sensors as follows:

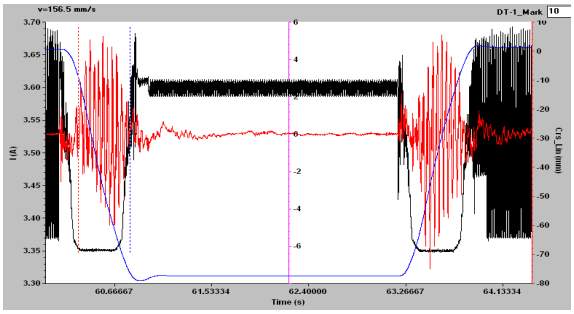

Figure 13: Medium speed movement (156.99 mm/s).

- The displacement sensor was connected at the robot's arm free end. The objective is to measure the total displacement realized by the end effector. Because of the sensor's intrinsic structure, and for obtaining a linear relation between sensor measurement and robot displacement in the 3D space, we restricted the robot's movement to a movement in a plane formed by the robot's backbone and the sensor's extension axis
- The accelerometer was placed in the same point as the displacement sensor. The objective is to determine the vibration induced in the robot arm structure by the actuation system and the control algorithm.
- The ammeter was connected in a serial mode with one of the stepper motor phases (the stepper motors are tree phases ones). The objective is to determine the stepper motor current need during the movements, and also to detect if and when the losing steps phenomenon occurs, based on the fact that a losing step process can be noticed by observing a high current peak.

In the figure 10 can be observed a recorded dataset. The measured current is represented with black color, with blue is represented the arm displacement, and with red is marked the oscillation recorded at the end of the robot arm. The dataset recorded a same trajectory described by the robot, but at different speeds. In the left side can be observed the movement execution at a lowest speed (19.23 mm/s), and in the right side at high speed (330 mm/s). In the following paragraphs we will analyze the robot's behavior for these two extreme movements. The first move observed was executed with a speed of 19.23 mm/s, going forward from the origin to the end point and, after a short break, back to the original. The detailed recorded data can be seen in the Figure 11.

The oscillation was amplified 100 times, for having a better view for its evolution. As expected for slow moves case, when the effort needed for robot arm displacement is low, the current evolution indicates that the stepper motor doesn't lose any steps and the movement there is no position error. Regarding oscillation, one can observe that near the origin position the robot exhibits a higher oscillation of its end effector. We consider that this phenomenon appeared due to the fact that near origin the tension in the actuation cables is lower, because the potential energy due gravity have the lowest value, and at end point the potential energy have a considerable higher value, conducting to a higher tension in cables which prevents the robot arm to oscillate.

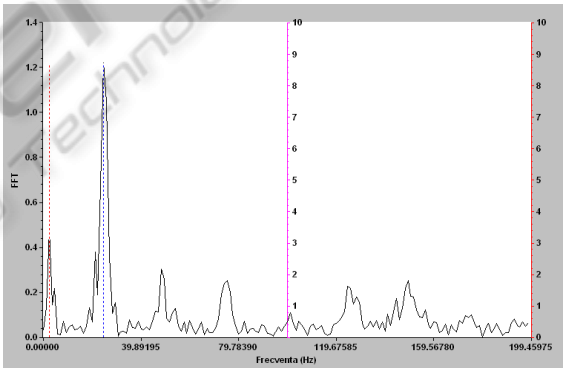

Figure 14: Frequency analysis for oscillation. Medium speed case.

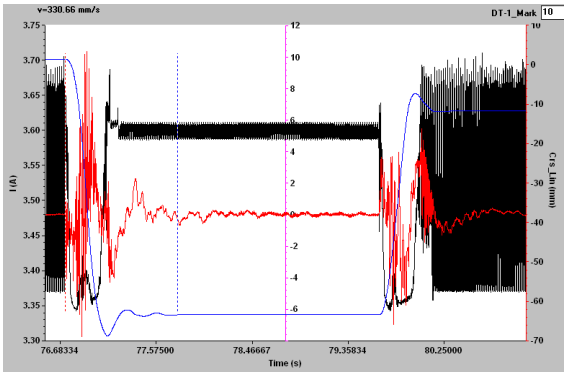

Figure 15: High speed movement.

If we take a closer look at the oscillation, and make a frequency analysis (figure 12), it can be observed that there are two spikes in frequency, one at 2.9 Hz, and one at 159.99 Hz.

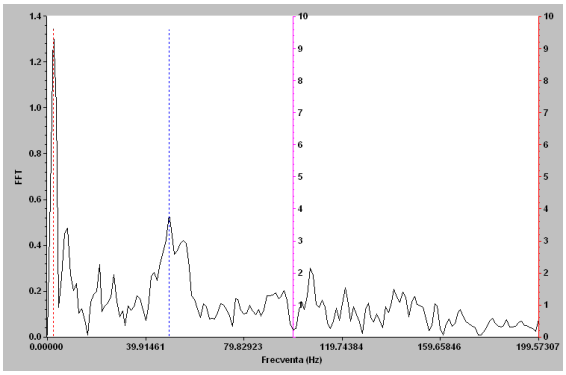

Figure 16: Frequency analysis for oscillation. High speed case.

As already identified, where an artificial vision system was used (Tanasie et al., 2009), the first spike at 2.9 Hz represents the natural resonance frequency for the robotic arm. By observing the oscillation analysis for faster movements, we determined that the second spike, with a higher level, placed at 159.99 Hz, is induced by the actuation system – the vibrations frequency generated by the actuation system and transmitted in the cables, also being responsible for the resonance spike at 2.9 Hz.

Considering a medium speed movement (156.99 mm/s), the following dataset was recorded (Figure 13). Analyzing the current evolution, a singular spike can be observed at 63.8 second on the timescale, which indicates that the motor loses a single step, this situation being caused by the fast stop of the robotic arm. Correlated with this fact, the analysis of the trajectory evolution shows that the end of the robot arm don't stop directly at the desired position, and under the effect of inertia determined by its own mass it passes that position. While the cables exhibit neither compression nor extension, the position error is determined exclusively by a shear effect. Shear is an elastic deformation, thus generating a force that brings the robot arm back at the desired position. This transitory effect takes 0.2 seconds and the maximum position error is 2 millimeters.

The oscillation graph shows a similar evolution as described for the previous case, but the frequency analysis gives a different characteristic (Figure 14). The natural oscillation frequency can be identified as a spike at the same frequency 2.9 Hz, but the vibration induced by the actuation system may be found now at 24.6 Hz, as a result of the motor's speed variation.

The last observed evolution is for high speed movement (330 mm/s). The recorded data is represented in the Figure 15. The current evolution is more dramatic and irregular, as can be observed in the figure 15 (marked with black line). The current profile isn't anymore smooth, as in previous cases, and some major fluctuations can be seen at 76.9 sec and at 79.7 sec. Those fluctuations correspond to a large number of lost steps, the effort required for moving the robot being very large. This conclusion is sustained by the conclusions of analysis conducted for displacement and vibration. Regarding the displacement, the robot was programmed to execute the very same movement, going from origin to a desired position and then back to the origin, but at different speeds. This means that in all recorded data, the robot must achieve the same desired position, and the position at the end of the movement must be the same with the position from where the movement started (the origin). Observing the displacement from figure 15 (marked with blue line), it can be determined a difference of 12 mm between the beginning position and final position. Also, if one compares the desired position achieved in figure 11, 13 and 15, can determine that the desired position is achieved successfully in figure 11 and 13, but in figure 15 the robot fails to reach the desired position, introducing a position error of 6 mm. The inertial effect is very high, the robot presenting a large oscillation before remaining steady in the desired position. Previous conclusions are also sustained by the recorded vibrations, marked with red line in figure 15. On the same timeline with the current fluctuations can be noticed a large amplitude of the vibration, as an effect of the discontinuity in movement determined by lost steps. Moreover, as the frequency analysis shown in the figure 16 denotes, this high speed actuation determines a resonance with the natural frequency of the robot arm, affecting the robot arm evolution.

5 CONCLUSIONS

As conclusions, for the slow speed moves, there are no lost steps in stepper motors, meaning that an open loop control can be successfully applied to the system. There is a low amplitude oscillation of the robot's arm, mainly at 159.99 Hz, induced by the actuation system, but it induces only a small

amplitude natural frequency resonance, so the robot arm doesn't resonate with actuation system. Also, considering the displacement (marked with blue in the figure), it can be observed that the position error is zero. The overall behavior of the structure is a very good one.

For the medium speed moves, the stepper motors may lose steps, but this phenomenon occurs occasionally and can be considered insignificant if is evaluated as a ratio lost steps / total number of steps, meaning that an open loop control can still be successfully applied to the system. There is a low amplitude oscillation of the robot's arm, mainly at 24.6 Hz, induced by the actuation system, but it induces only a small amplitude natural frequency resonance, so the robot arm doesn't resonate with actuation system. The displacement record reveals a transient evolution around the final position, introducing a transient position error, having 2 mm maximum amplitude and with a short duration, 0.2 seconds. At the end of the transient evolution, the robot stops on the desired position and the position error is zero. The overall behavior of the structure is a good one.

ACKNOWLEDGEMENTS

The research presented in this paper was supported by the Romanian National University Research Council CNCSIS through the IDEI Research Grant ID93 and by FP6 MARTN through FREESUBNET Project no. 36186.

REFERENCES

Blessing, M., Walker, I. D., 2004. Novel Continuum Robots with Variable- Length Sections, Proceedings 3rd IFAC Symposium on Mechatronic Systems, Sydney, Australia, September 2004, pp. 55-60.

Boccolato, G., Manta, F., Dumitru, S., Cojocaru, D., 2009. 3D Control for a Tentacle Robot, 3rd International Conference on Applied Mathematics, Simulation, Modelling (ASM'09), Vouliagmeni Beach, Athens, Greece.

Cojocaru, D., Tanasie, R. T., Marghitu, D. B., 2008. A Complex Mathematical Expression Operations Tool, Annals of The Univ. of Craiova, Series: Automation, Computers, Electronics And Mechatronics, ISSN: 1841-0626, Volume 5(32), no. 1, pp. 7-12.

Cowan, L. S. and Walker, I. D., 2008. "Soft" Continuum Robots: the Interaction of Continuous and Discrete Elements, Artificial Life XI.

Crespi, A. and Ijspeert, A. J., 2006. An amphibious snake robot that crawls and swims using a central pattern generator. 9th International Conference on Climbing and Walking Robots (CLAWAR 2006), pp19-27.

Dumitru, S., Cojocaru, D., Dumitru, N., Ciupitu, I., Geonea, I., Dumitru, V., 2009. Finite Element Modeling of a Polyarticulated Robotic System, Annals of DAAAM, ISSN 1726-9679, pp 969.

Ivanescu, M., Cojocaru, D., Popescu, N., Popescu, D., Tănasie, R.T., 2006. Hyperredundant Robot Control by Visual Servoing, Studies in Informatics and Control Journal, Volume 15, Number 1, pp93-102, ISSN 1220-1766.

Robinson, G., Davies, J. B. C., 1999. Continuum robots—A state of the art. IEEE International Conference on Robotics and Automation, pp2849–2854. Detroit, MI.

Suzumori, K., Iikura, S., Tanaka, H., 1991. Development of Flexible Microactuator and its application to Robotic Mechanisms, Proceedings of the IEEE International Conference on Robotics and Automation, pp. 1622-1627.

Tanasie, R. T., Ivanescu, M., Cojocaru, D., 2009. Camera Positioning and Orienting for Hyperredundant Robots Visual Servoing Applications, Journal of Control Engineering and Applied Informatics, Vol 11, No 1, p19-26, ISSN 1454-8658.